



# Time-resolved characterization of primary particle emissions and secondary particle formation from a modern gasoline passenger car

Panu Karjalainen<sup>1</sup>, Hilikka Timonen<sup>2</sup>, Erkkka Saukko<sup>1</sup>, Heino Kuuluvainen<sup>1</sup>, Sanna Saarikoski<sup>2</sup>, Päivi Aakko-Saksa<sup>3</sup>, Timo Murtonen<sup>3</sup>, Matthew Bloss<sup>2</sup>, Miikka Dal Maso<sup>1</sup>, Pauli Simonen<sup>1</sup>, Erik Ahlberg<sup>4,5</sup>, Birgitta Svenningsson<sup>5</sup>, William Henry Brune<sup>6</sup>, Risto Hillamo<sup>2</sup>, Jorma Keskinen<sup>1</sup>, and Topi Rönkkö<sup>1</sup>

<sup>1</sup>Aerosol Physics Laboratory, Department of Physics, Tampere University of Technology, P.O. Box 692, 33101 Tampere, Finland

<sup>2</sup>Atmospheric Composition Research, Finnish Meteorological Institute, P.O. Box 503, 00101, Helsinki, Finland

<sup>3</sup>VTT Technical Research Centre of Finland Ltd., P.O. Box 1000, 02044 VTT, Espoo, Finland

<sup>4</sup>Centre for Environmental and Climate research, Lund University, Box 118, 22100 Lund, Sweden

<sup>5</sup>Division of Nuclear Physics, Lund University, Box 118, 22100 Lund, Sweden

<sup>6</sup>Department of Meteorology, Pennsylvania State University, University Park, PA, USA

Correspondence to: Topi Rönkkö (topi.ronkko@tut.fi)

Received: 10 November 2015 – Published in Atmos. Chem. Phys. Discuss.: 25 November 2015

Revised: 23 May 2016 – Accepted: 21 June 2016 – Published: 14 July 2016

**Abstract.** Changes in vehicle emission reduction technologies significantly affect traffic-related emissions in urban areas. In many densely populated areas the amount of traffic is increasing, keeping the emission level high or even increasing. To understand the health effects of traffic-related emissions, both primary (direct) particulate emission and secondary particle formation (from gaseous precursors in the exhaust emissions) need to be characterized. In this study, we used a comprehensive set of measurements to characterize both primary and secondary particulate emissions of a Euro 5 level gasoline passenger car. Our aerosol particle study covers the whole process chain in emission formation, from the tailpipe to the atmosphere, and also takes into account differences in driving patterns. We observed that, in mass terms, the amount of secondary particles was 13 times higher than the amount of primary particles. The formation, composition, number and mass of secondary particles was significantly affected by driving patterns and engine conditions. The highest gaseous and particulate emissions were observed at the beginning of the test cycle when the performance of the engine and the catalyst was below optimal. The key parameter for secondary particle formation was the amount of gaseous hydrocarbons in primary emissions; however, also the primary particle population had an influence.

## 1 Introduction

Vehicular emissions deteriorate the air quality locally (Wehner et al., 2002; Pirjola et al., 2012; Lähde et al., 2014) and contribute significantly to the air pollution levels in urban areas. Air pollution components like particulate matter contribute to adverse health effects of people (e.g., Pope III and Dockery, 2006). The human exposure to pollutants in urban environments is the highest in the vicinity of traffic. In order to reduce the adverse health effects and exposure of people by pollutants, the emission regulation for vehicles with direct injection engines include limits for particulate mass (PM), and in Europe for some vehicle types, particle number (PN) (Dieselnet, 2016), of which the PN limit is considered to be stricter. Limits for gaseous compounds cover total hydrocarbon emissions, nitrogen oxides and carbon monoxide. Both particulate and gaseous emissions are strongly affected by technology development (e.g., catalysts and filters), driven by legislation activities. This technology development also has, in general, other effects than required by emission legislation; for example, fuel sulfur content limitations affect the emissions of nanoparticles. It should be noted that, e.g., semi-volatile compounds (e.g., low-volatility organics, sulfuric compounds) are not directly regulated even though they are partially detected in the gravimetric PM determination as

particles or adsorbed gas phase artefacts (Chase et al., 2004; Höglström et al., 2012). Although not directly regulated, low-volatility organics are likely to be affected by gaseous hydrocarbon limits.

In the gasoline vehicle fleet, the port-fuel injection (PFI) techniques has been widely replaced by gasoline direct injection (GDI) technologies due to the need to decrease fuel consumption and  $\text{NO}_x$  emissions of passenger cars (e.g., Alkidas, 2007; CARB, 2010). The disadvantage of GDI technologies is the increased primary particle emission (Aakko and Nylund, 2003; Mohr et al., 2006; Braisher et al., 2010). The GDI vehicle exhaust particle number concentrations are typically significantly lower than the diesel exhaust particle concentrations without a diesel particulate filter (DPF) but higher than concentrations with a DPF (Mathis et al., 2005). The GDI engine exhaust particle size distribution has been observed to be bimodal (Barone et al., 2012; Sementa et al., 2012; Sgro et al., 2012; Maricq et al., 1999; Karjalainen et al., 2014; Pirjola et al., 2015a) and the emission is dominated by elemental carbon (EC) (Maricq et al., 2012). Organic carbon (OC) constitutes only a small fraction of particle emissions. Particles are (in number) mainly in ultrafine sizes (e.g., Maricq et al., 1999; Harris and Maricq, 2001; Khalek et al., 2010; Karjalainen et al., 2014). According to the study of Karjalainen et al. (2014), the GDI exhaust particles can be divided into four different types: spherical amorphous particles consisting of carbon with mean particle size between 10 and 20 nm (see also Sgro et al., 2012; Barone et al., 2012); agglomerated soot-like particles with mean particle size between 30 and 60 nm; lubricant oil originating particles consisting of metallic ash components (Rönkkö et al., 2014); and semivolatile nucleation particles (see also Mathis et al., 2005; Li et al., 2013). The highest emissions of primary particles take place under acceleration and deceleration conditions (Karjalainen et al., 2014).

Secondary aerosol formation happens in the atmosphere through oxidation processes that tend to lower the saturation vapor pressures of organic species. Thus, more oxidized compounds, mostly organic compounds, are more likely found in the particle phase (Robinson et al., 2007). Fresh exhaust emissions contain a variety of different organic compounds, in the scale of hundreds or thousands of different components (Rogge et al., 1993). Part of those have low saturation vapor pressure already when emitted and thus they are observed in primary particulate emission or in particulate phase after the exhaust has been diluted rapidly into the atmospheric conditions (Tobias et al., 2001; Sakurai et al., 2003; Arnold et al., 2012; Pirjola et al., 2015b). However, even the majority of organic compounds in the exhaust are primarily emitted to the atmosphere in the gaseous phase. Also, sulfur compounds such as  $\text{SO}_2$ , as well as nitrogen oxides, can play a role in the secondary aerosol formation processes in the atmosphere.

There are studies of engine-exhaust-related secondary organic aerosol (SOA) formation for gasoline (Suarez-Bertoa

et al., 2015; Nordin et al., 2013; Platt et al., 2013; Gordon et al., 2014) and diesel vehicles (e.g., Weitkamp et al., 2007; Chirico et al., 2010; Gordon et al., 2013). In these, the secondary particulate emissions of gasoline vehicles have been studied using a smog chamber so that diluted exhaust gas has been led to the smog chamber during a test cycle, a constant speed operation or idling condition (Chirico et al., 2010; Nordin et al., 2013). However, in the emission's perspective, this represents only the average over the test, and more detailed analysis of the effect of driving pattern and engine conditions on SOA formation is lacking. With the potential aerosol mass (PAM) concept (Kang et al., 2007, 2011) SOA emissions can be studied in a shorter timescale (minutes). The PAM is a flow-through-type reactor that uses UV lamps to form oxidants ( $\text{O}_3$ , OH,  $\text{HO}_2$ ). Secondary aerosol formation processes are accelerated so that a few minutes' residence time corresponds to the atmospheric aging of several days or even weeks. In principle, the PAM reactor enables real-time measurements of secondary particulate emissions during the driving cycle. The PAM concept has been previously applied in vehicular exhaust studies, e.g., by Tkacik et al. (2014) who used the reactor in a traffic tunnel to study the secondary aerosol properties, and by Pourkhesalian et al. (2015) who used the PAM reactor in connection with diesel exhaust particle volatility and reactive oxygen species (ROS) studies. High oxidant concentrations, (100–1000 times atmospheric concentrations of  $\text{O}_3$ , OH,  $\text{HO}_2$ ) and UV lights used in the chamber are shown to simulate SOA formation in the atmosphere (Kang et al., 2007, 2011). The aging as the sample flows through the chamber is shown to represent several days' aging in the atmosphere (Kang et al., 2011; Ortega et al., 2013).

In this work, the aim is to show how the driving conditions of modern gasoline vehicles affect the emissions, especially the secondary particulate emission. To meet this goal, comprehensive set of real-time instruments was used to study the physical and chemical characteristics of primary and secondary particle emissions as well as gaseous emissions of a modern GDI passenger car. The sampling of exhaust for primary emission measurements was conducted by mimicking the real-world atmospheric dilution. Secondary emission was studied by using a PAM reactor designed to mimic atmospheric aging of aerosol. Experiments were performed for the official European test cycle for passenger cars that is the New European Driving Cycle (NEDC). Special attention was paid to the temporal behavior of primary and secondary particle emissions, e.g., emissions during the engine cold start and in different driving patterns.

## 2 Materials and methods

The test vehicle was a modern gasoline passenger car (model year 2011, 1.4L turbo-charged GDI engine, 7-gear dual clutch automatic transmission, weight 1557 kg, odometer

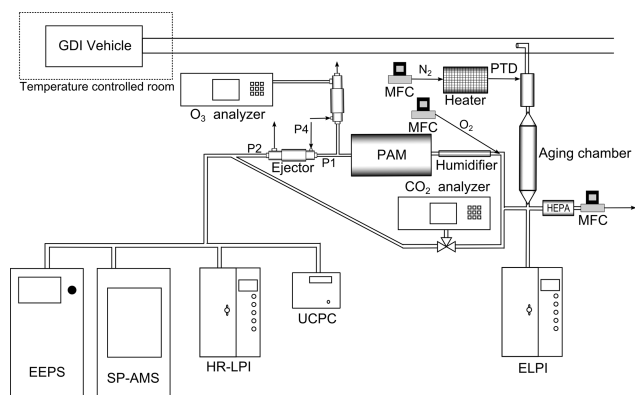


**Figure 1.** Schematic of the experimental setup (MFC = mass flow controller).

reading 48 700 km, emission level Euro 5 with a 3-way catalytic converter). Test fuels comprised of regular commercial E10 (max 10 % ethanol) with sulfur content being below 10 ppm. The driving cycle used in the study was New European Driving Cycle (NEDC) (Fig. 2a). The European exhaust emissions driving cycle NEDC is defined in the UN ECE R83 regulation. The car was tested on a chassis dynamometer in a climatic test cell at +23 °C. NEDC totals 11.0 km, here divided into three test phases to study emissions at cold start and with warmed-up engines. The first and second test phases (later called as cold start urban driving cycle, CSUDC, and hot urban driving cycle, HUDC) each consisted of 2.026 km driving, and the third test phase, the extra-urban driving cycle (EUDC), was 6.955 km.

As shown in Fig. 1, particle sampling was conveyed by a partial exhaust sampling system (Ntziachristos et al., 2004) at thermally insulated and externally heated exhaust transfer lines (stainless steel AISI 316L). The sampling system consisted of a porous tube diluter (PTD) (dilution ratio (DR) 12, dilution nitrogen temperature 30 °C), residence time chamber (2.5 s) and secondary dilution conducted by Dekati diluter (DR 8). In terms of exhaust nucleation particle formation, the sampling system mimics the real exhaust dilution and nanoparticle formation processes in the atmosphere (Rönkkö et al., 2006; Keskinen and Rönkkö, 2010).

A potential aerosol mass (PAM) chamber is a small flow through chamber developed to simulate aerosol aging in the atmosphere. The PAM chamber was installed between the aging chamber and secondary dilution units of sampling system. PAM chamber is thoroughly described by Kang et al. (2007, 2011) and Lambe et al. (2011, 2015). Shortly, PAM chamber is a stainless steel cylinder (length 46 cm, diameter 22 cm, volume  $\sim$  13 L). In an effort to reduce wall effects, the PAM flow reactor was designed with a larger radial/axial dimension ratio and a smaller surface-to-volume ratio relative to other flow reactors (Lambe et al., 2011; Kang et al., 2011). Two UV lamps (BHK Ink., Ca) were used to produce oxidants ( $O_3$ , OH and  $HO_2$ ) as well as

UV light (185, 254 nm). The sample flow through the PAM chamber was set to  $\sim 9.75 \text{ L min}^{-1}$  resulting average residence time of 84 s. Voltage of the two UV lamps was at maximum value, 190 V. Relative humidity (RH) and temperature were measured prior to the PAM with stable values of 60 % and 22 °C, respectively. Typically, ozone concentration after the PAM was on average 6 ppm. The PAM chamber was calibrated using average experiment conditions and following the same procedure described by Lambe et al. (2011). The corresponding OH exposure was calculated to be  $1.03 \times 10^{12} \text{ molec. cm}^{-3} \text{ s}$ , representing approximately 8 days of aging in the atmosphere.

PAM chamber has been used in different ambient environments (Palm et al., 2016; Ortega et al., 2016; Tkacik et al., 2014) and also thoroughly characterized in the laboratory conditions via measurements and modeling (e.g., Lambe et al., 2011, 2015; Peng et al., 2015; Ortega et al., 2013). The oxidant concentrations in the PAM chamber are higher (100–1000 times) than in the atmosphere (Kang et al., 2007); however, the ratios between oxidants are similar to the atmosphere. Several studies (e.g., Kang et al., 2007, 2011) have compared PAM results to atmospheric results. Kang et al. (2007, 2011) showed that the yields of OA from individual organic precursor gases were similar to those obtained in large environmental chambers and that the extent of OA oxidation appears to be similar to that observed in the atmosphere and greater than that observed in large environmental chambers and laboratory flow tubes. Also, according to results of Tkacik et al. (2014), the chemical evolution of the organic aerosol in the PAM reactor is similar to that observed in the atmospheric measurements. Additionally, Tkacik et al. (2014) observed that the mass spectrum of the unoxidized primary organic aerosol closely resembles ambient hydrocarbon-like organic aerosol (HOA) and that aged PM firstly resembles semivolatile oxygenated organic aerosol (SV-OOA) and then low-volatility organic aerosol (LV-OOA) at higher OH exposures. In this study, cycles were firstly run without the PAM chamber to measure primary emissions and secondly with the PAM chamber in order to study the formation of secondary particulate material. Before the experiment, the PAM chamber was cleaned by running pure  $N_2$ - $O_2$  mixture with UV lights on.

Transmission efficiency of gases (CO and  $SO_2$ ) in the PAM chamber has shown that wall losses in the PAM chamber are very small (Lambe et al., 2011). Primary particle losses for a PAM chamber (results shown in Fig. S1 in the Supplement) are in general small especially in the particle sizes that contain most of the aerosol mass: 25 % at 50 nm, 15 % at 100 nm and below 10 % above 150 nm.

The particle instrumentation was located downstream of the secondary diluter. The particle size distributions were measured on-line (1 Hz time resolution) with a high-resolution low-pressure impactor (HRLPI) (Arffman et al., 2014), fitted into an ELPI bodywork to replace the original charger and impactor, and an engine exhaust particle sizer

(EEPS, TSI Inc.) (Johnson et al., 2004). The particle number concentration was also measured with an ultrafine condensation particle counter (UCPC, TSI Inc. model 3025) that was located downstream of a passive nanoparticle diluter (DR 42). A SP-AMS was used to measure chemical composition (ions, organic carbon, refractory black carbon and some metals) of emitted submicron (50–800 nm) particulate matter (PM).

SP-AMS is a high-resolution time-of-flight aerosol mass spectrometer (HR-ToF-AMS) with added laser (intracavity Nd:YAG, 1064 nm) vaporizer (Schwarz et al., 2008). The HR-ToF-AMS is described in detail by DeCarlo et al. (2006) and Jayne et al. (2000), and SP-AMS is described by Onasch et al. (2012) and Schwarz et al. (2008). Briefly, in the SP-AMS an aerodynamic lens is used to form a narrow beam of particles that is transmitted into the detection chamber, where the species are flash vaporized. Particles are vaporized either by a normal tungsten vaporizer at 600 °C to analyze inorganic ion and OC concentrations or with an SP laser (intracavity Nd:YAG, 1064 nm) in order to analyze black carbon and metals. The vaporized compounds are ionized using electron impact ionization (70 eV). Ions formed are guided to the time-of-flight chamber. A multi-channel plate (MCP) is used as a detector. The time resolution of AMS measurements was 5 s. The 1 min detection limits for submicrometer particles are  $< 0.04 \mu\text{g m}^{-3}$  for all species in the V mode. The IGOR 6.11 (Wavemetrics, Lake Oswego, OR), Squirrel 1.53 (Sueper, 2013) and PIKA 1.12F were used to analyze the SP-AMS data. Elemental analysis (based on Aiken et al., 2008) was performed on the HR-ToF-AMS data to determine the aerosol hydrogen-to-carbon (H/C) and oxygen-to-carbon (O/C) ratios. CO<sub>2</sub> concentrations during the measurement period were significantly higher (up to 1450 ppm) than atmospheric values (400 ppm), thus CO<sub>2</sub> time series was used to correct the artefact caused by gaseous CO<sub>2</sub>. Collection efficiency (CE) value represents the fraction of sampled particle mass that is detected by the detector and CE value is needed for the calculation of aerosol mass concentration measured by the AMS. Previous studies have shown that the CE of SP-AMS is affected by (i) particle losses during transit through the inlet and lens, (ii) the particle beam divergence for both tungsten and laser vaporizers and for tungsten vaporizer also due to (iii) bounce effects from the vaporizer (Huffman et al., 2009; Matthew et al., 2008; Onasch et al., 2012). It is known that in the standard AMS with only the tungsten vaporizer the CE can depend on the chemical composition and acidity of aerosol as well as sampling relative humidity (Middlebrook et al., 2012), the default value for the CE being 0.5. For the SP-AMS, the CE can vary significantly from the default value of 0.5 due to the laser vaporizer. Onasch et al. (2012) estimated collection efficiency of coated black particles in the SP-AMS to be 0.75, whereas Willis et al. (2014) measured CE = 0.6 for bare regal black (typically used as a surrogate for BC in laboratory) particles but they observed a significant increase in CE with increas-

ing coating thickness. A CE of 1 was used in this study for all SP-AMS data. We acknowledge that it is likely that the collection efficiency might be overestimated (and calculated mass concentrations underestimated) for uncoated, primary emissions, whereas for heavily coated spherical secondary aerosol, the CE is probably closer to its real value. Due to the low contribution of inorganic species, it was not relevant to use the method of Middlebrook et al. (2012) for estimating the CE.

Equipment used in the measurement of the CO, HC, and NO<sub>x</sub> emissions conforms to the specifications of the Directive 70/220/EEC and its amendments. The true oxygen contents and densities of the fuels were used in the calculation of the results. A flame ionization detector (FID) was used for the measurement of hydrocarbons (all carbon-containing compounds, also oxygenates) (Sandström-Dahl et al., 2010; Aakko-Saksa et al., 2014). The calculation method chosen uses the density of  $619 \text{ kg m}^{-3}$  (different from the EC regulation 692/2008). A number of gaseous compounds (19 in total), nitrogen dioxide (NO<sub>2</sub>), ammonia (NH<sub>3</sub>), nitrous oxide (N<sub>2</sub>O), ethanol, formaldehyde and acetaldehyde, amongst others, were measured on-line with 2 s time resolution using Fourier transformation infrared (FTIR) equipment (Gasmeter Cr-2000).

The analysis of OH exposure and non-OH chemistry was performed with the calculator tool developed by Peng et al. (2016). The inputs to the model are humidity, OH reactivity (OHR) and photon flux or ozone concentrations. The OHR is estimated based on volatile organic compound (VOC) and CO measurements. During the measurements, there were PVF bags that were analyzed for VOCs of special interest for gasoline vehicles with gas chromatograph (HP 5890 Series II, AL2O<sub>3</sub>, KCl/PLOT column, an external standard method). Separate samples were analyzed for CSUDC, HUDC and EUDC, and these results are presented Table S2 in the Supplement. To find the total external (input) OHR, the sum of all analyzed concentrations (VOCs and CO) multiplied with the corresponding rate constants (Atkinson and Arey, 2003) was calculated.

### 3 Results and discussion

#### 3.1 Primary particulate and gaseous emissions of gasoline passenger car

##### 3.1.1 Particle size distributions

The driving cycle used in the study was NEDC, a statutory cycle in emission testing in Europe. The cycle consists of several patterns describing typical driving in urban environments and highway driving (Fig. 2a), with the total duration and length of the cycle 1200 s and 11.0 km, respectively. Figure 2 shows the speed of the test vehicle during the test cycle and particle number concentration, particle volume concen-

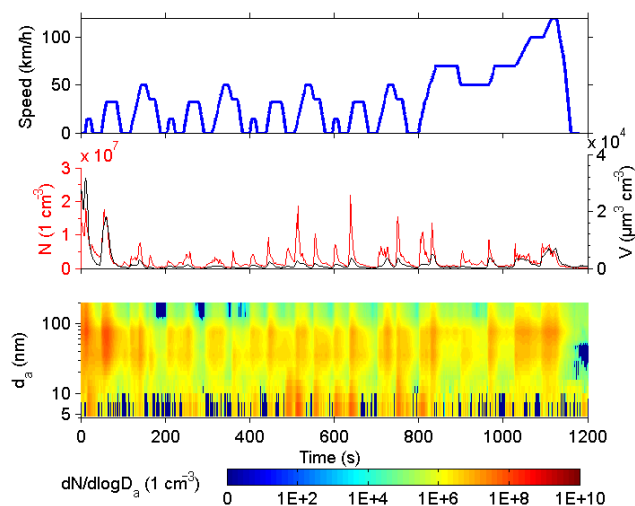


**Figure 2.** Speed profile, primary particle number (measured by the CPC) and volume concentrations (measured by HRLPI) and primary particle size distributions (HRLPI) for the studied gasoline passenger car during the NEDC test cycle.

tration and particle size distribution of vehicle exhaust, all measured with high time resolution (1 s).

The exhaust particle number concentration was strongly dependent on driving condition (Fig. 1b). Large particle number concentrations were observed during accelerations, especially during the first two accelerations when the engine had not yet reached steady temperature conditions, and they were therefore associated with high engine loading and altering combustion conditions. In addition to soot particles (particle diameters of 30–100 nm, see Fig. 1c), there were also frequent observations of small particles ( $D_p < 10$  nm), especially in the middle part of the cycle. These nanoparticles are most likely associated with deceleration and engine braking conditions (Rönkkö et al., 2014; Karjalainen et al., 2014). The largest particle volume concentrations were observed at the beginning, just after ignition and, on the other hand, at the end of the test cycle when the driving was at high speed and engine load. High total particle volume concentrations were strongly linked with the existence of soot-mode particles in the exhaust.

### 3.1.2 Chemical composition

Figure 3 shows the chemical composition of primary exhaust particles during the NEDC cycle. The lower pane shows the major components, revealing that the large particle emission at the beginning of the cycle consists mainly of organic compounds and refractory black carbon (rBC). When compared to Fig. 2, it can be seen that the organic compounds together with rBC form the so-called soot mode, which dominates the particle volume concentration due to its large particle size. While the rBC has formed in the engine due to the incomplete combustion of fuel-forming agglomerated soot parti-

cles (Heywood, 1988), the organic compounds have likely been condensed onto the soot particle surface mainly during cooling dilution process of exhaust. Figure 3 shows that later, after the starting phase of the test cycle, the relative concentration of rBC decreases and remains at low levels with the exception of the accelerations at the highway part of the cycle. Interestingly, the concentration of organic compounds was very significant in the middle part of the cycle, i.e., when the emissions of nanoparticles (see Fig. 2) were observed to be high. Thus, while the high emission of organic compounds seems to be linked with high soot/rBC emission at the beginning of the cycle, in the middle part the organics and rBC emissions seemed not to be interlinked.

Concentrations of inorganic species ( $\text{SO}_4$ ,  $\text{NH}_4$ ,  $\text{NO}_3$ , Cl) are shown in the upper pane of Fig. 3. Note that the concentration axes differ. In general, the highest sulfate and nitrate concentrations existed during accelerations, and had a good correlation with soot/rBC emissions. The sulfate concentration increases also during certain periods in the middle part of the cycle, clearly linked with similar peaks in organic compounds concentration (see Fig. 3). Interestingly, during highway driving and the following deceleration, significant concentration of ammonium, nitrate and chloride ions were also observed.

### 3.1.3 Gaseous emissions

The time series of total hydrocarbons, ammonia and  $\text{NO}_x$  during the NEDC test cycle are presented in Fig. 4. The largest hydrocarbon emissions were observed at beginning of the cycle due to low engine and exhaust gas temperatures, which lowers the efficiency of the oxidation process in the three-way catalytic converter, in addition to higher formation rates of gaseous hydrocarbons during combustion. The hydrocarbon emissions are in line with the measurements of the chemical composition of particles, which shows that the highest emissions of particulate organic compounds occur at the beginning of the cycle. However, during the middle part of the cycle, the emissions of gaseous hydrocarbons and organic particulate matter did not correlate; although in particle phase organics (see Fig. 3) the concentrations reached high values also during middle part of the cycle, the gaseous hydrocarbons remained at very low level until the highway driving part of the cycle. The  $\text{NO}_x$  emissions were the highest at the beginning of the cycle and during the last part of the cycle when the driving speed and combustion temperatures were high. Ammonia concentrations were at the level of 10 ppm during most of the cycle; concentration even higher than 100 ppm was measured during the accelerations at the end of the cycle. The highest ammonia concentrations were clearly linked with acceleration, under conditions when the air-to-fuel ratio can be below 1 (rich mixture). This is in line with the findings by Mejia-Centeno et al. (2007) and Heeb et al. (2006), showing ammonia formation in the three-way cat-

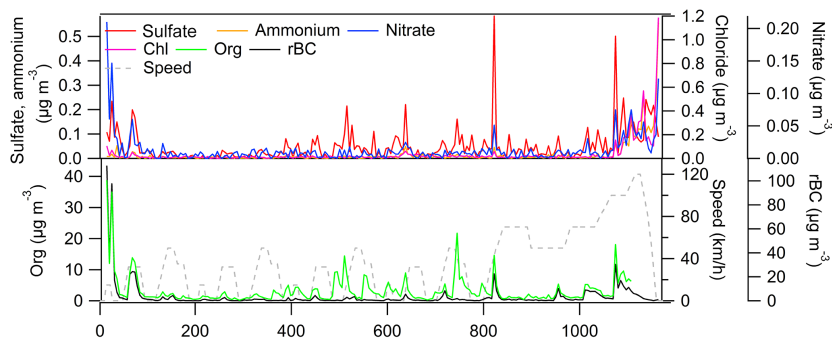


**Figure 3.** Temporal behavior of rBC, organics,  $\text{SO}_4$ ,  $\text{NO}_3$  and  $\text{NH}_4$  concentrations measured by the SP-AMS for the primary emissions (without the PAM chamber) during the NEDC test cycle.

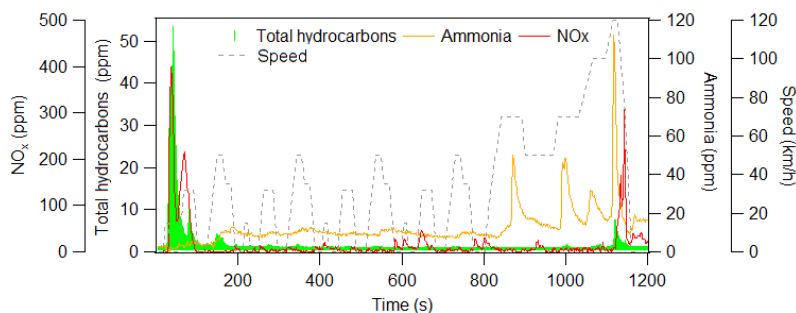


**Figure 4.** Time series of the exhaust concentrations of total hydrocarbons, ammonia and  $\text{NO}_x$ .

alyst in slightly rich air-to-fuel ratios, which are prevailing during acceleration.

### 3.2 Secondary particle formation from a gasoline passenger car

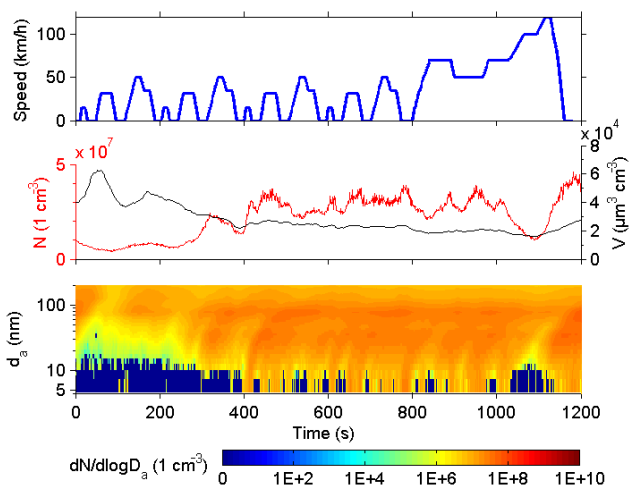
#### 3.2.1 Particle size distributions

Figure 4 shows the secondary particle number concentrations, volume concentrations and size distributions of gasoline passenger car exhaust during the NEDC cycle. In general, the volume and number concentrations as well as mean particle size of secondary particles were significantly larger than those of the primary particles, throughout the cycle. Periodic behavior similar to that of the primary particles can be observed: first, a period with large soot-mode particles, then a period with a large number of small nanoparticles and finally the highway part of the cycle.

As shown above, after the ignition, the emissions of gaseous precursors (hydrocarbons and nitrogen-containing species) and primary particles were observed to be high (Fig. 4). This, combined with the information in Fig. 5, indicates that the existence of gaseous precursors in the exhaust significantly increases the secondary particulate matter formation, resulting in a high volume concentration of large particles at the beginning of the test cycle (Fig. 5). Compared to other periods of the cycle, at the beginning the vol-

ume concentration of secondary particles was 3 times higher, highlighting the role of cold starts in total secondary particle emission of gasoline vehicles.

The high oxidant concentrations in the PAM chamber result also in high concentrations of condensing compounds, which causes a possibility for nucleation in the chamber. In this study, we measured higher particle number concentrations for the sample treated by the PAM than for the untreated sample. However, the increase of particle number was not very significant and, in principle, may also be caused by the increase of particle size into the measurement range on aerosol instruments. Interestingly, nanoparticles were not observed in the primary emission during the first period of cycle (Fig. 2), when both the precursor gas concentration and resulted volume of secondary particulate matter was the highest. During the first period, the mean particle number concentrations were also on a relatively similar level, both in the primary and secondary aerosol. Instead, nanoparticles were observed in the sample treated by the PAM during the second phase (starting at 400 s) of the cycle. During this part of the test cycle the nanoparticles existed also in primary emissions. Thus, the results indicate that nanoparticles found after PAM chamber are obviously initially formed, already before the sample was introduced into the PAM chamber. It should be kept in mind that the existence and growth of nanoparticles in the PAM chamber can slightly change the mean particle size and thus how effectively they are detected by aerosol instru-



**Figure 5.** Speed profile, secondary particle number (measured by the CPC) and volume concentrations (measured by the HRLPI) and secondary particle number size distributions (HRLPI) for the studied gasoline passenger car during the NEDC test cycle.

ments; e.g., the particle size range of aerosol mass spectrometers does not typically cover particles smaller than 50 nm, and in several studies the particle number size distribution measurement is limited to sizes above 10 nm.

As stated above, in the middle part of the cycle, a large number of primary nanoparticles was introduced into the chamber from the exhaust. Figure 4 shows that these sub-5 nm particles grew in the chamber to particle sizes similar to primary soot particles. This takes approximately 60–80 s, corresponding to the mean residence time in the PAM. In general, it seems that both the primary soot particles and primary nanoparticles can have an important role in secondary particle formation dynamics resulting, e.g., in the size distribution of aged exhaust aerosol.

### 3.2.2 Chemical composition of secondary particles

The secondary aerosol mass consisted mainly of organic compounds and rBC (Fig. 6, lower panel). At the beginning of the test cycle, the concentrations of organic compounds in the secondary particulate matter were about 100 times higher than their concentrations in primary particles, while the O : C ratio dipped below 0.5 (see Fig. S3). During other parts of the cycle, the concentrations of the organic compounds were significantly lower and remained relatively stable. The rBC concentration level did not change significantly because rBC is a primary component.

At the beginning of the cycle, the incomplete combustion causes high emissions of rBC and gaseous hydrocarbons. Simultaneously, the temperature of the three-way catalyst is low and thus the reduction of hydrocarbons is not optimal. In the PAM reactor, the oxidation of hydrocarbons lowers their volatility, which results in high emissions of secondary par-

ticulate matter consisting of organic compounds. During the highway part of the cycle, the incomplete combustion again causes the emission of soot/rBC during certain acceleration phases. However, during the highway part, the temperature of the catalyst used in the vehicle is very high, approximately 700 °C (see Karjalainen et al., 2014), meaning that it keeps the emissions of gaseous hydrocarbon emissions at a very low level. Thus, during the highway part the concentration of organic precursors is low in the exhaust, resulting in a low concentration of secondary organic particulate material.

In addition to rBC and organic compounds, during the middle part of the cycle the concentrations of inorganic species were observed to be stable. Only a slight increase in sulfate concentration was observed, simultaneously with the existence of nanoparticles in secondary aerosol. This observation is in line with primary particle measurements where sulfate peaks were observed during the middle part of the cycle. During the highway part of the cycle the concentrations of inorganic species in the secondary particulate matter increases when compared to the previous parts of the cycle. This is seemingly caused by high emissions of gaseous nitrogen compounds (see Fig. 4). Results indicate that also these compounds may have a significant role in traffic-related secondary aerosol formation. However, this kind of aerosol is very specifically formed only at high vehicle speeds.

### 3.2.3 Influence of driving conditions to emission characteristics

The results presented above indicate that both the primary and secondary emissions vary strongly as a function of the driving cycle. To clarify the effects of driving conditions on the concentrations of secondary and primary particles, the cycle was divided into three sections according to the engine and speed profile conditions: CSUDC (0–391 s), HUDC (392–787 s) and EUDC (788–1180 s). The CSUDC represents the cold start situation, the HUDC represents typical city driving with a warm engine and the EUDC represents typical highway driving. Figure 7 shows chemical composition and O : C ratios of primary and secondary (primary components excluded) exhaust particles for these three sections. O : C ratios were determined for organic compounds based on chemical composition measured by the SP-AMS, so that inorganic species and rBC were excluded. Emission factors for measured compounds are presented in the Supplement (see Fig. S4 and Table S1).

Primary particle emissions were dominated by rBC and organics. It should be noted that although the CSUDC and HUDC were similar from the viewpoint of driving conditions, the rBC concentration was 4 times higher during CSUDC. Again, during the EUDC section of the cycle higher rBC concentration was observed in the exhaust. In contrast, for the organics, similar differences between the sections of the test cycle were not observed. Inorganic species concen-

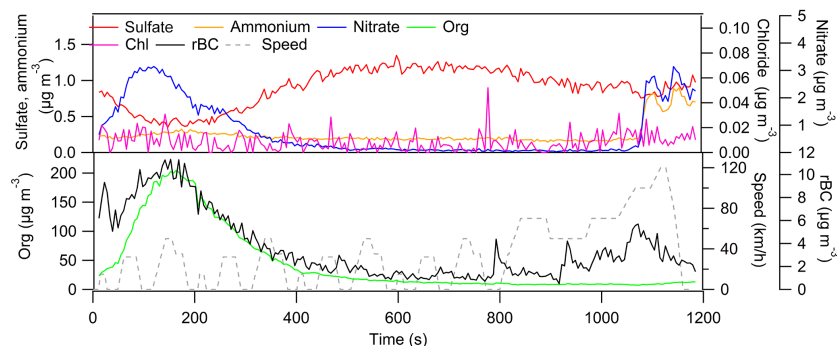


**Figure 6.** Temporal behavior of rBC, organics,  $\text{SO}_4$ ,  $\text{NO}_3$ ,  $\text{NH}_4$  and Cl concentrations measured by the SP-AMS downstream of the PAM chamber during the NEDC test cycle.

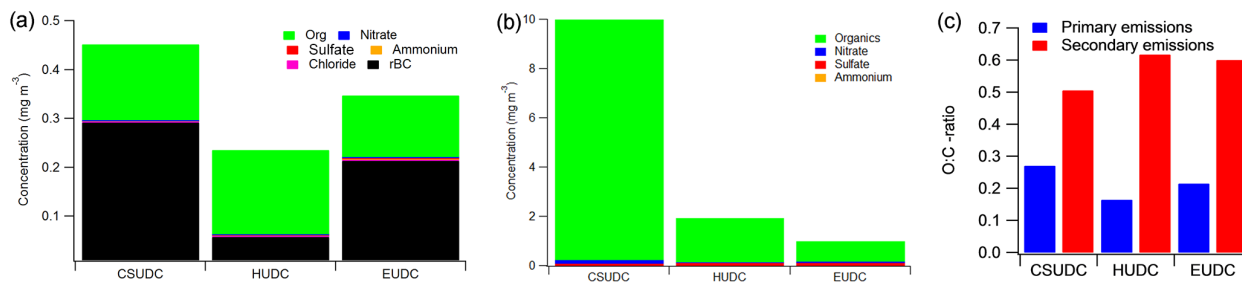


**Figure 7.** (a) Chemical composition of primary PM, (b) chemical composition secondary PM and (c) the O:C ratios of primary and secondary particulate matter for different parts of the NEDC cycle.

trations were relatively low in all cycle sections representing on average 3.6 % of particulate mass.

On average, the secondary particulate emissions were 13 times higher than the primary particle emissions. This value is higher or at similar level than observed in previous studies. For instance, Suarez-Bertoa et al. (2015) reported 2–4 times higher values for the secondary particle emissions of gasoline vehicles when compared to the primary organics and BC. In the diesel exhaust study of Chirico et al. (2010), the secondary and primary particle emissions were at similar levels. However, in the study of Platt et al. (2013) SOA emission was around 14 times higher than primary organic aerosol (POA) emission when they measured the emissions of gasoline vehicles for the NEDC cycle. All of these studies were conducted using a batch chamber, while in our study a flow-through chamber was used. The differences between the studies can be due to the differences in the emissions but also due to the differences in wall losses, exhaust and oxidant concentrations and photochemical ages.

The chemical composition of secondary particles differed significantly from primary particles; in secondary particles most of the particulate matter consisted of organics, in primary particles the role of rBC was significant. The calculated secondary organics concentration was high especially during CSUDC, even  $9.9 \text{ mg m}^{-3}$ . This highlights the important role of primary and secondary emissions followed by the cold

start. It should be noted that the emission factors of both primary and secondary particles were lowest during the EUDC (see the Supplement).

O:C ratios were relatively stable for primary emissions; slightly higher O:C ratio (0.27) was observed for the CSUDC. Similar O:C ratios have been typically observed for fresh traffic emissions in urban ambient measurements (Timonen et al., 2013; Carbone et al., 2014). For the secondary emissions, the O:C ratios were between 0.5 and 0.6. Large hydrocarbon emissions and probably differences in oxidation levels of primary gaseous compounds at the beginning of the cycle, as well as differences in oxidant levels in chamber are likely reasons for observed differences. Previous studies for gasoline vehicles reported high O:C ratios (up to 0.7) for secondary organic exhaust aerosol (Suarez-Bertoa et al., 2015; Platt et al., 2013) but also lower ratios of  $\sim 0.4$  (Nordin et al., 2013).

With all input parameters determined, the OH exposure and VOC fate in the PAM was calculated based on the Peng et al. (2016) model. Much higher OHR values were observed followed by the cold start. OHR, on average, for the CSUDC based on the measured compounds was around  $1000 \text{ s}^{-1}$  (Table S2) which is overall a riskier condition according to Peng et al. (2016). This means that about 30 % of total loss of toluene and benzene is due to photolysis at 185 nm, but for all other measured compounds the non-OH chemistry and pho-

tolysis are minor or very minor (Peng et al., 2016, calculator in the Supplement). For the HUDC and EUDC OHRs were 15 and  $56\text{ s}^{-1}$ , respectively, indicating very minor photolysis and non-OH chemistry.

The average OH exposure during the CSUDC was approximately  $1.2 \times 10^{11}\text{ molec. cm}^{-3}\text{ s}$  according to the model. This is about an order of magnitude lower than during  $\text{SO}_2$  calibration experiments ( $1.03 \times 10^{12}\text{ molec. cm}^{-3}\text{ s}$ , measured from  $\text{SO}_2$  concentrations) where OHR was significantly lower, about  $2\text{ s}^{-1}$ . This indicates that during the experiment OH exposure varied roughly in the scale of  $10^{11}$ – $10^{12}\text{ molec. cm}^{-3}\text{ s}$  (1–8 days equivalent atmospheric aging) depending on the exhaust pollutant levels.

#### 4 Conclusions

In this study, we characterized primary particle and gaseous emissions and secondary particle formation from a Euro 5 emission level direct injection gasoline vehicle. All the measurements were made in real time with high time resolution. Measurements were conducted under driving conditions representing typical urban driving cycles. Our aim was to create a basis for understanding the links between driving conditions, primary emissions of aerosols and their precursors and the formation of secondary particulate material. We approached this issue by using a potential aerosol mass (PAM) chamber enabling the characterization of secondary emissions in real time, combined with comprehensive characterization of PM and gaseous compounds.

Our results indicated higher- or similar-level secondary particulate matter emissions compared to the previous studies (Suarez-Bertoa et al., 2015; Platt et al., 2013). Compared to primary particle emissions, our study indicated 13 times higher secondary particulate emissions, dominated by organics. The study of Suarez-Bertoa et al. (2015) indicated 2–4 times higher emissions for secondary particles, instead, in the study of Platt et al. (2013) SOA emission was around 9–15 times higher than POA emission for the NEDC cycle. For reference, the primary particle emissions measured in this study were at similar levels than in previous studies for modern gasoline vehicles (Karjalainen et al., 2014).

We observed that during ignition and during the first few minutes of the test cycle, i.e., when the engine and the catalyst had not reached normal operation temperatures, the emissions of primary PM and precursor gases were the largest and therefore a large amount of secondary organic emission was formed. This was the case even though in the PAM chamber external OH reactivity was high after the cold start, and photolysis degradation for some VOCs was partially active. The following similar driving cycle with a warmed engine produced significantly lower primary and secondary particulate emissions. This indicates that the adverse effects of traffic are likely to be largest in city areas where driving distances are typically short, near houses and

workplaces. However, we note that the formation of secondary particulate matter is a longer-time atmospheric process and thus not directly linked with human exposure and human health at the site of emission. Also, it is reasonable to assume that this problem, at least from the viewpoint of secondary aerosol precursor emissions, is magnified under cold climatic conditions.

Both primary and secondary emissions were highly dependent on driving conditions such as speed, acceleration and deceleration profiles. At high speed (EUDC), both particulate mass and size distribution were different when compared to low-speed driving (HUDC). In addition, under deceleration conditions, very small nanoparticles were observed in primary exhaust. These nanoparticles grew in particle size due to the condensation of highly oxidized engine origin compounds. These oxidized compounds were formed in our experiment in the PAM chamber but when forming in the atmosphere they likely exhibit similar behavior and prefer to condense on the nanoparticles. Thus, our results indicate that also nanoparticles can contribute to atmospheric secondary aerosol formation, especially on size distribution of secondary particles. Due to that, it is clear that current legislation focusing on larger particles (PM mass or number of particles larger than 23 nm in diameter) is not optimal from the viewpoint of realistic urban air quality, since it takes into account only the largest primary particles.

#### 5 Data availability

The data of this study are available from the authors upon request.

**The Supplement related to this article is available online at doi:10.5194/acp-16-8559-2016-supplement.**

*Acknowledgements.* We acknowledge support by Tekes (the Finnish Funding Agency for Technology and Innovation), Cleen Ltd (MMEA project), the Academy of Finland (Grant no. 259016), IEA-AMF Annex 44 and the Swedish Research Councils VR and Formas.

Edited by: G. McFiggans

Reviewed by: three anonymous referees

#### References

- Aakko, P. and Nylund, N.-O.: Particle Emissions at Moderate and Cold Temperatures Using Different Fuels, *Soc. Automot. Eng.*, SP-1809(724), 279–296, doi:10.4271/2003-01-3285, 2003.
- Aakko-Saksa, P., Rantanen-Kolehmainen, L., and Skyttä, E.: Ethanol, Isobutanol, and Biohydrocarbons as Gasoline

- Components in Relation to Gaseous Emissions and Particulate Matter, *Environ. Sci. Technol.*, 48, 10489–10496, doi:10.1021/es501381h, 2014.
- Aiken, A. C., DeCarlo, P. F., Kroll, J. H., Worsnop, D. R., Huffman, J. A., Docherty, K., Ulbrich, I. M., Mohr, C., Kimmel, J. R., Sueper, D., Sun, Y., Zhang, Q., Trimborn, A., Northway, M., Ziemann, P. J., Canagaratna, M. R., Onasch, T. B., Alfarra, M. R., Prevot, A. S. H., Dommen, J., Duplissy, J., Metzger, A., Baltensperger, U., and Jiménez, J. L.: O / C and OM / OC Ratios of Primary, Secondary, and Ambient Organic Aerosols with a High Resolution Time-of-Flight Aerosol Mass Spectrometer, *Environ. Sci. Technol.*, 42, 4478–4485, 2008.
- Alkidas, A. C.: Combustion advancements in gasoline engines, *Energy Convers. Manag.*, 48, 2751–2761, doi:10.1016/j.enconman.2007.07.027, 2007.
- Arffman, A., Yli-Ojanperä, J., Kalliokoski, J., Harra, J., Pirjola, L., Karjalainen, P., Rönkkö, T., and Keskinen, J.: High-resolution low-pressure cascade impactor, *J. Aerosol Sci.*, 78, 97–109, doi:10.1016/j.jaerosci.2014.08.006, 2014.
- Arnold, F., Pirjola, L., Rönkkö, T., Reichl, U., Schlager, H., Lähde, T., Heikkilä, J., and Keskinen, J.: First online measurements of sulfuric acid gas in modern heavy-duty diesel engine exhaust: implications for nanoparticle formation, *Environ. Sci. Technol.*, 46, 11227–11234, doi:10.1021/es302432s, 2012.
- Atkinson, R. and Arey, J.: Atmospheric degradation of volatile organic compounds., *Chem. Rev.*, 103, 4605–38, doi:10.1021/cr0206420, 2003.
- Barone, T. L., Storey, J. M. E., Youngquist, A. D., and Szybist, J. P.: An analysis of direct-injection spark-ignition (DISI) soot morphology, *Atmos. Environ.*, 49, 268–274, doi:10.1016/j.atmosenv.2011.11.047, 2012.
- Braisher, M., Stone, R., and Price, P.: Particle Number Emissions from a Range of European Vehicles, *Soc. Automot. Eng.*, 13 pp., doi:10.4271/2010-01-0786, 2010.
- CARB: Proposed amendments to Californias low-emission vehicle regulations – particulate matter mass, ultrafine solid particle number, and black carbon emissions, Workshop report, California Air Resources Board, 2010.
- Carbone, S., Aurela, M., Saarnio, K., Saarikoski, S., Timonen, H., Frey, A., Sueper, D., Ulbrich, I. M., Jimenez, J. L., Kulmala, M., Worsnop, D. R., and Hillamo, R. E.: Wintertime Aerosol Chemistry in Sub-Arctic Urban Air, *Aerosol Sci. Technol.*, 48, 313–323, doi:10.1080/02786826.2013.875115, 2014.
- Chase, R. E., Duszakiewicz, G. J., Richert, J. F. O., Lewis, D., Maricq, M. M., and Xu, N.: PM Measurement Artifact: Organic Vapor Deposition on Different Filter Media, *SAE Int.*, 11 pp., doi:10.4271/2004-01-0967, 2004.
- Chirico, R., DeCarlo, P. F., Heringa, M. F., Tritscher, T., Richter, R., Prévôt, A. S. H., Dommen, J., Weingartner, E., Wehrle, G., Gysel, M., Laborde, M., and Baltensperger, U.: Impact of aftertreatment devices on primary emissions and secondary organic aerosol formation potential from in-use diesel vehicles: results from smog chamber experiments, *Atmos. Chem. Phys.*, 10, 11545–11563, doi:10.5194/acp-10-11545-2010, 2010.
- DeCarlo, P. F., Kimmel, J. R., Trimborn, A., Northway, M. J., Jayne, J. T., Aiken, A. C., Gonin, M., Fuhrer, K., Horvath, T., Docherty, K. S., Worsnop, D. R., and Jimenez, J. L.: Field-Deployable, High-Resolution, Time-of-Flight Aerosol Mass Spectrometer, *Anal. Chem.*, 78, 8281–8289, doi:10.1021/ac061249n, 2006.
- Dieselnet: available at: <http://www.dieselnet.com/>, last access: 7 March 2016.
- Gordon, T. D., Tkacik, D. S., Presto, A. A., Zhang, M., Jathar, S. H., Nguyen, N. T., Massetti, J., Truong, T., Cicero-Fernandez, P., Maddox, C., Rieger, P., Chattopadhyay, S., Maldonado, H., Maricq, M. M., and Robinson, A. L.: Primary gas- and particle-phase emissions and secondary organic aerosol production from gasoline and diesel off-road engines, *Environ. Sci. Technol.*, 47, 14137–46, doi:10.1021/es403556e, 2013.
- Gordon, T. D., Presto, A. A., May, A. A., Nguyen, N. T., Lipsky, E. M., Donahue, N. M., Gutierrez, A., Zhang, M., Maddox, C., Rieger, P., Chattopadhyay, S., Maldonado, H., Maricq, M. M., and Robinson, A. L.: Secondary organic aerosol formation exceeds primary particulate matter emissions for light-duty gasoline vehicles, *Atmos. Chem. Phys.*, 14, 4661–4678, doi:10.5194/acp-14-4661-2014, 2014.
- Harris, S. J. and Maricq, M. M.: Signature size distributions for diesel and gasoline engine exhaust particulate matter, *J. Aerosol Sci.*, 32, 749–764, doi:10.1016/S0021-8502(00)00111-7, 2001.
- Heeb, N. V., Forss, J. A-M., Brühlmann, S., Lüscher, R., Saxer, C. J., and Hug, P.: Correlation of hydrogen, ammonia and nitrogen monoxide (nitric oxide) emissions of gasoline-fueled Euro-3 passenger cars at transient driving, *Atmos. Environ.*, 40, 3750–3763, doi:10.1016/j.atmosenv.2006.03.002, 2006.
- Heywood, J. B.: *Internal Combustion Engine Fundamentals*, 932 pp., McGraw-Hill, 1988.
- Högström, R., Karjalainen, P., Yli-Ojanperä, J., Rostedt, A., Heinonen, M., Mäkelä, J. M., and Keskinen, J.: Study of the PM Gas-Phase Filter Artifact Using a Setup for Mixing Diesel-Like Soot and Hydrocarbons, *Aerosol Sci. Tech.*, 46, 1045–1052, doi:10.1080/02786826.2012.689118, 2012.
- Huffman, J. A., Docherty, K. S., Mohr, C., Cubison, M. J., Ulbrich, I. M., Ziemann, P. J., Onasch, T. B., and Jimenez, J. L.: Chemically-Resolved Volatility Measurements of Organic Aerosol from Different Sources, *Environ. Sci. Technol.*, 43, 5351–5357, doi:10.1021/es803539d, 2009.
- Jayne, J. T., Leard, D. C., Zhang, X., Davidovits, P., Smith, K. A., Kolb, C. E. and Worsnop, D. R.: Development of an Aerosol Mass Spectrometer for Size and Composition Analysis of Submicron Particles, *Aerosol Sci. Tech.*, 33, 49–70, doi:10.1080/027868200410840, 2000.
- Johnson, T., Caldow, R., Pocher, A., Mirmem, A., and Kittelson, D.: A New Electrical Mobility Particle Sizer Spectrometer for Engine Exhaust Particle Measurements, 2004-01-13, *SAE Pap.*, 2004.
- Kang, E., Root, M. J., Toohey, D. W., and Brune, W. H.: Introducing the concept of Potential Aerosol Mass (PAM), *Atmos. Chem. Phys.*, 7, 5727–5744, doi:10.5194/acp-7-5727-2007, 2007.
- Kang, E., Toohey, D. W., and Brune, W. H.: Dependence of SOA oxidation on organic aerosol mass concentration and OH exposure: experimental PAM chamber studies, *Atmos. Chem. Phys.*, 11, 1837–1852, doi:10.5194/acp-11-1837-2011, 2011.
- Karjalainen, P., Pirjola, L., Heikkilä, J., Lähde, T., Tzamkiozis, T., Ntziachristos, L., Keskinen, J., and Rönkkö, T.: Exhaust particles of modern gasoline vehicles: a laboratory and an on-road study, *Atmos. Environ.*, 97, 262–270, doi:10.1016/j.atmosenv.2014.08.025, 2014.
- Keskinen, J. and Rönkkö, T.: Can Real-World Diesel Exhaust Particle Size Distribution be Reproduced in the Laboratory?

- A Critical Review, *J. Air Waste Manage.*, 60, 1245–1255, doi:10.3155/1047-3289.60.10.1245, 2010.
- Khalek, I. A., Bougher, T., and Jetter, J. J.: Particle Emissions from a 2009 Gasoline Direct Injection Engine Using Different Commercially Available Fuels, *SAE Int. J. Fuels Lubr.*, 3, 623–637, doi:10.4271/2010-01-2117, 2010.
- Lähde, T., Niemi, J. V., Kousa, A., Rönkkö, T., Karjalainen, P., Keskinen, J., Frey, A., Hillamo, R., and Pirjola, L.: Mobile Particle and NO<sub>x</sub> Emission Characterization at Helsinki Downtown: Comparison of Different Traffic Flow Areas, *Aerosol Air Qual. Res.*, 14, 1372–1382, doi:10.4209/aaqr.2013.10.0311, 2014.
- Lambe, A. T., Ahern, A. T., Williams, L. R., Slowik, J. G., Wong, J. P. S., Abbatt, J. P. D., Brune, W. H., Ng, N. L., Wright, J. P., Croasdale, D. R., Worsnop, D. R., Davidovits, P., and Onasch, T. B.: Characterization of aerosol photooxidation flow reactors: heterogeneous oxidation, secondary organic aerosol formation and cloud condensation nuclei activity measurements, *Atmos. Meas. Tech.*, 4, 445–461, doi:10.5194/amt-4-445-2011, 2011.
- Lambe, A. T., Chhabra, P. S., Onasch, T. B., Brune, W. H., Hunter, J. F., Kroll, J. H., Cummings, M. J., Brogan, J. F., Parmar, Y., Worsnop, D. R., Kolb, C. E., and Davidovits, P.: Effect of oxidant concentration, exposure time, and seed particles on secondary organic aerosol chemical composition and yield, *Atmos. Chem. Phys.*, 15, 3063–3075, doi:10.5194/acp-15-3063-2015, 2015.
- Li, T., Chen, X., and Yan, Z.: Comparison of fine particles emissions of light-duty gasoline vehicles from chassis dynamometer tests and on-road measurements, *Atmos. Environ.*, 68, 82–91, doi:10.1016/j.atmosenv.2012.11.031, 2013.
- Maricq, M., Podsiadlik, D., Brehob, D., and Haghgooe, M.: Particulate Emissions from a Direct-Injection Spark-Ignition (DISI) Engine, *SAE Tech. Pap. Ser.*, 1999.
- Maricq, M. M., Szente, J. J., and Jahr, K.: The Impact of Ethanol Fuel Blends on PM Emissions from a Light-Duty GDI Vehicle, *Aerosol Sci. Tech.*, 46, 576–583, doi:10.1080/02786826.2011.648780, 2012.
- Mathis, U., Mohr, M., and Forss, A.: Comprehensive particle characterization of modern gasoline and diesel passenger cars at low ambient temperatures, *Atmos. Environ.*, 39, 107–117, doi:10.1016/j.atmosenv.2004.09.029, 2005.
- Matthew, B. M., Middlebrook, A. M., and Onasch, T. B.: Collection Efficiencies in an Aerodyne Aerosol Mass Spectrometer as a Function of Particle Phase for Laboratory Generated Aerosols, *Aerosol Sci. Tech.*, 42, 884–898, doi:10.1080/02786820802356797, 2008.
- Mejia-Centeno, I., Martínez-Hernández, A., and Fuentes, G.: Effect of low-sulfur fuels upon NH<sub>3</sub> and N<sub>2</sub>O emission during operation of commercial three-way catalytic converters. *Topics in Catalysis*, 42–43, 381–385, doi:10.1007/s11244-007-0210-2, 2007.
- Middlebrook, A. M., Bahreini, R., Jimenez, J. L., and Canagaratna, M. R.: Evaluation of Composition-Dependent Collection Efficiencies for the Aerodyne Aerosol Mass Spectrometer using Field Data, *Aerosol Sci. Tech.*, 46, 258–271, doi:10.1080/02786826.2011.620041, 2012.
- Mohr, M., Forss, A., and Lehmann, U.: Particle emissions from diesel passenger cars equipped with a particle trap in comparison to other technologies, *Environ. Sci. Technol.*, 40, 2375–2383, doi:10.1021/es051440z, 2006.
- Nordin, E. Z., Eriksson, A. C., Roldin, P., Nilsson, P. T., Carlsson, J. E., Kajos, M. K., Hellén, H., Wittbom, C., Rissler, J., Löndahl, J., Swietlicki, E., Svenningsson, B., Bohgard, M., Kulmala, M., Hallquist, M., and Pagels, J. H.: Secondary organic aerosol formation from idling gasoline passenger vehicle emissions investigated in a smog chamber, *Atmos. Chem. Phys.*, 13, 6101–6116, doi:10.5194/acp-13-6101-2013, 2013.
- Ntziachristos, L., Giechaskiel, B., Pistikopoulos, P., Samaras, Z., Mathis, U., Mohr, M., Ristimäki, J., Keskinen, J., Mikkanen, P., Casati, R., Scheer, V., and Vogt, R.: Performance evaluation of a novel sampling and measurement system for exhaust particle characterization, 2004-01-14, *SAE 2004 World Congr. Exhib.*, 2004.
- Onasch, T. B., Trimborn, A., Fortner, E. C., Jayne, J. T., Kok, G. L., Williams, L. R., Davidovits, P., and Worsnop, D. R.: Soot Particle Aerosol Mass Spectrometer: Development, Validation, and Initial Application, *Aerosol Sci. Tech.*, 46, 804–817, 2012.
- Ortega, A. M., Day, D. A., Cubison, M. J., Brune, W. H., Bon, D., de Gouw, J. A., and Jimenez, J. L.: Secondary organic aerosol formation and primary organic aerosol oxidation from biomass-burning smoke in a flow reactor during FLAME-3, *Atmos. Chem. Phys.*, 13, 11551–11571, doi:10.5194/acp-13-11551-2013, 2013.
- Ortega, A. M., Hayes, P. L., Peng, Z., Palm, B. B., Hu, W., Day, D. A., Li, R., Cubison, M. J., Brune, W. H., Graus, M., Warneke, C., Gilman, J. B., Kuster, W. C., de Gouw, J., Gutiérrez-Montes, C., and Jimenez, J. L.: Real-time measurements of secondary organic aerosol formation and aging from ambient air in an oxidation flow reactor in the Los Angeles area, *Atmos. Chem. Phys.*, 16, 7411–7433, doi:10.5194/acp-16-7411-2016, 2016.
- Palm, B. B., Campuzano-Jost, P., Ortega, A. M., Day, D. A., Kaser, L., Jud, W., Karl, T., Hansel, A., Hunter, J. F., Cross, E. S., Kroll, J. H., Peng, Z., Brune, W. H., and Jimenez, J. L.: In situ secondary organic aerosol formation from ambient pine forest air using an oxidation flow reactor, *Atmos. Chem. Phys.*, 16, 2943–2970, doi:10.5194/acp-16-2943-2016, 2016.
- Peng, Z., Day, D. A., Ortega, A. M., Palm, B. B., Hu, W. W., Stark, H., Li, R., Tsigaridis, K., Brune, W. H., and Jimenez, J. L.: Non-OH chemistry in oxidation flow reactors for the study of atmospheric chemistry systematically examined by modeling, *Atmos. Chem. Phys. Discuss.*, 15, 23543–23586, doi:10.5194/acpd-15-23543-2015, 2015.
- Peng, Z., Day, D. A., Ortega, A. M., Palm, B. B., Hu, W., Stark, H., Li, R., Tsigaridis, K., Brune, W. H., and Jimenez, J. L.: Non-OH chemistry in oxidation flow reactors for the study of atmospheric chemistry systematically examined by modeling, *Atmos. Chem. Phys.*, 16, 4283–4305, doi:10.5194/acp-16-4283-2016, 2016.
- Pirjola, L., Lähde, T., Niemi, J. V., Kousa, A., Rönkkö, T., Karjalainen, P., Keskinen, J., Frey, A., and Hillamo, R.: Spatial and temporal characterization of traffic emissions in urban microenvironments with a mobile laboratory, *Atmos. Environ.*, 63, 156–167, doi:10.1016/j.atmosenv.2012.09.022, 2012.
- Pirjola, L., Karjalainen, P., Heikkilä, J., Saari, S., Tzamkiozis, T., Ntziachristos, L., Kulmala, K., Keskinen, J., and Rönkkö, T.: Effects of Fresh Lubricant Oils on Particle Emissions Emitted by a Modern Gasoline Direct Injection Passenger Car, *Environ. Sci. Technol.*, 49, 3644–3652, doi:10.1021/es505109u, 2015a.
- Pirjola, L., Karl, M., Rönkkö, T., and Arnold, F.: Model studies of volatile diesel exhaust particle formation: are organic vapours

- involved in nucleation and growth?, *Atmos. Chem. Phys.*, 15, 10435–10452, doi:10.5194/acp-15-10435-2015, 2015b.
- Platt, S. M., El Haddad, I., Zardini, A. A., Clairotte, M., Astorga, C., Wolf, R., Slowik, J. G., Temime-Roussel, B., Marchand, N., Ježek, I., Drinovec, L., Mocnik, G., Möhler, O., Richter, R., Barmet, P., Bianchi, F., Baltensperger, U., and Prévôt, A. S. H.: Secondary organic aerosol formation from gasoline vehicle emissions in a new mobile environmental reaction chamber, *Atmos. Chem. Phys.*, 13, 9141–9158, doi:10.5194/acp-13-9141-2013, 2013.
- Pope III, C. A. and Dockery, D. W.: Critical Review: Health Effects of Fine Particulate Air Pollution: Lines That Connect, *J. Air Waste Manage.*, 56, 709–742, 2006.
- Pourkhesalian, A. M., Stevanovic, S., Rahman, M. M., Faghihi, E. M., Bottle, S. E., Masri, A. R., Brown, R. J., and Ristovski, Z. D.: Effect of atmospheric aging on volatility and reactive oxygen species of biodiesel exhaust nano-particles, *Atmos. Chem. Phys.*, 15, 9099–9108, doi:10.5194/acp-15-9099-2015, 2015.
- Robinson, A. L., Donahue, N. M., Shrivastava, M. K., Weitkamp, E. A., Sage, A. M., Grieshop, A. P., Lane, T. E., Pierce, J. R., and Pandis, S. N.: Rethinking Organic Aerosols: Semivolatile Emissions and Photochemical Aging, *Science*, 315, 1259–1262, doi:10.1126/science.1133061, 2007.
- Rogge, W. F., Hildemann, L. M., Mazurek, M. A., Cass, G. R., and Simoneit, B. R. T.: Sources of fine organic aerosol. 2. Noncatalyst and catalyst-equipped automobiles and heavy-duty diesel trucks, *Environ. Sci. Technol.*, 27, 636–651, doi:10.1021/es00041a007, 1993.
- Rönkkö, T., Virtanen, A., Vaaraslahti, K., Keskinen, J., Pirjola, L. and Lappi, M.: Effect of dilution conditions and driving parameters on nucleation mode particles in diesel exhaust: Laboratory and on-road study, *Atmos. Environ.*, 40, 2893–2901, doi:10.1016/j.atmosenv.2006.01.002, 2006.
- Rönkkö, T., Pirjola, L., Ntziachristos, L., Heikkilä, J., Karjalainen, P., Hillamo, R., and Keskinen, J.: Vehicle engines produce exhaust nanoparticles even when not fueled., *Environ. Sci. Technol.*, 48, 2043–2050, doi:10.1021/es405687m, 2014.
- Sakurai, H., Tobias, H. J., Park, K., Zarling, D., Docherty, K. S., Kittelson, D. B., McMurry, P. H., and Ziemann, P. J.: On-line measurements of diesel nanoparticle composition and volatility, *Atmos. Environ.*, 37, 1199–1210, doi:10.1016/S1352-2310(02)01017-8, 2003.
- Sandström-Dahl, C., Erlandsson, L., Gasste, J., and Lindgren, M.: Measurement Methodologies for Hydrocarbons, Ethanol and Aldehyde Emissions from Ethanol Fuelled Vehicles, *SAE Int. J. Fuels Lubr.*, 3, 453–466, doi:10.4271/2010-01-1557, 2010.
- Schwarz, J. P., Spackman, J. R., Fahey, D. W., Gao, R. S., Lohmann, U., Stier, P., Watts, L. A., Thomson, D. S., Lack, D. A., Pfister, L., Mahoney, M. J., Baumgardner, D., Wilson, J. C., and Reeves, J. M.: Coatings and their enhancement of black carbon light absorption in the tropical atmosphere, *J. Geophys. Res.-Atmos.*, 113, 1–10, doi:10.1029/2007JD009042, 2008.
- Sementa, P., Maria Vaglieco, B., and Catapano, F.: Thermodynamic and optical characterizations of a high performance GDI engine operating in homogeneous and stratified charge mixture conditions fueled with gasoline and bio-ethanol, *Fuel*, 96, 204–219, doi:10.1016/j.fuel.2011.12.068, 2012.
- Sgro, L. A., Sementa, P., Vaglieco, B. M., Rusciano, G., D’Anna, A., and Minutolo, P.: Investigating the origin of nuclei particles in GDI engine exhausts, *Combust. Flame*, 159, 1687–1692, doi:10.1016/j.combustflame.2011.12.013, 2012.
- Suarez-Bertoa, R., Zardini, A. A., Keuken, H., and Astorga, C.: Impact of ethanol containing gasoline blends on emissions from a flex-fuel vehicle tested over the Worldwide Harmonized Light duty Test Cycle (WLTC), *Fuel*, 143, 173–182, doi:10.1016/j.fuel.2014.10.076, 2015.
- Sueper, D.: Data Analysis Updates for AMS-ToF (Squirrel 1.53 & Pika 1.12), AMS Users Meeting, 9 September 2013, available at: <http://cires1.colorado.edu/jjimenez-group/UsrMtg/UsersMtg14/SquirrelPika2013UsersMtg.pdf> (last access: 12 July 2016), 2013.
- Timonen, H., Carbone, S., Aurela, M., Saarnio, K., Saarikoski, S., Ng, N. L., Canagaratna, M. R., Kulmala, M., Kerminen, V. M., Worsnop, D. R., and Hillamo, R.: Characteristics, sources and water-solubility of ambient submicron organic aerosol in springtime in Helsinki, Finland, *J. Aerosol Sci.*, 56, 61–77, doi:10.1016/j.jaerosci.2012.06.005, 2013.
- Tkacik, D. S., Lambe, A. T., Jathar, S., Li, X., Presto, A. A., Zhao, Y., Blake, D., Meinardi, S., Jayne, J. T., Croteau, P. L., and Robinson, A. L.: Secondary organic aerosol formation from in-use motor vehicle emissions using a potential aerosol mass reactor, *Environ. Sci. Technol.*, 48, 11235–11242, doi:10.1021/es502239v, 2014.
- Tobias, H. J., Beving, D. E., Ziemann, P. J., Sakurai, H., Zuk, M., McMurry, P. H., Zarling, D., Waytulonis, R., and Kittelson, D. B.: Chemical analysis of diesel engine nanoparticles using a nano-DMA/thermal desorption particle beam mass spectrometer, *Environ. Sci. Technol.*, 35, 2233–2243, 2001.
- Wehner, B., Birmili, W., Gnauk, T., and Wiedensohler, A.: Particle number size distributions in a street canyon and their transformation into the urban-air background: Measurements and a simple model study, *Atmos. Environ.*, 36, 2215–2223, doi:10.1016/S1352-2310(02)00174-7, 2002.
- Weitkamp, E. A., Sage, A. M., Pierce, J. R., Donahue, N. M., and Robinson, A. L.: Organic aerosol formation from photochemical oxidation of diesel exhaust, *Environ. Sci. Technol.*, 41, 6969–6975, 2007.
- Willis, M. D., Lee, A. K. Y., Onasch, T. B., Fortner, E. C., Williams, L. R., Lambe, A. T., Worsnop, D. R., and Abbatt, J. P. D.: Collection efficiency of the soot-particle aerosol mass spectrometer (SP-AMS) for internally mixed particulate black carbon, *Atmos. Meas. Tech.*, 7, 4507–4516, doi:10.5194/amt-7-4507-2014, 2014.